Stem Cell Reports, Volume *9*

Supplemental Information

Hippocampal TERT Regulates Spatial Memory Formation through Modulation of Neural Development

Qi-Gang Zhou, Meng-Ying Liu, Han-Woong Lee, Fuyuki Ishikawa, Sushil Devkota, Xin-Ru Shen, Xin Jin, Hai-Yin Wu, Zhigang Liu, Xiao Liu, Xun Jin, Hai-Hui Zhou, Eun Jeoung Ro, Jing Zhang, Yu Zhang, Yu-Hui Lin, Hoonkyo Suh, and Dong-Ya Zhu

Supplementary Information

Hippocampal TERT regulates spatial memory formation through modulation of neural development

Qi-Gang Zhou, Meng-Ying Liu, Han-Woong Lee, Fuyuki Ishikawa, Sushil Devkota, Xin-Ru Shen, Xin Jin, Hai-Yin Wu, Zhigang Liu, Xiao Liu, Xun Jin, Hai-Hui Zhou, Eun Jeoung Ro, Jing Zhang, Yu Zhang, Yu-Hui Lin, Hoonkyo Suh, Dong-Ya Zhu

Supplemental Figures

Figure S1. Validation of the *Tert* $^{-/-}$ mice. Related to Figure 1

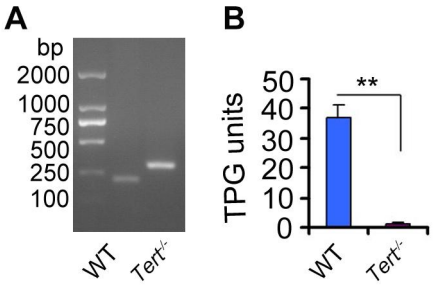

Figure S2. Latency to the platform in visible platform training**.** Related to Figure 1, 2, 6 and 7

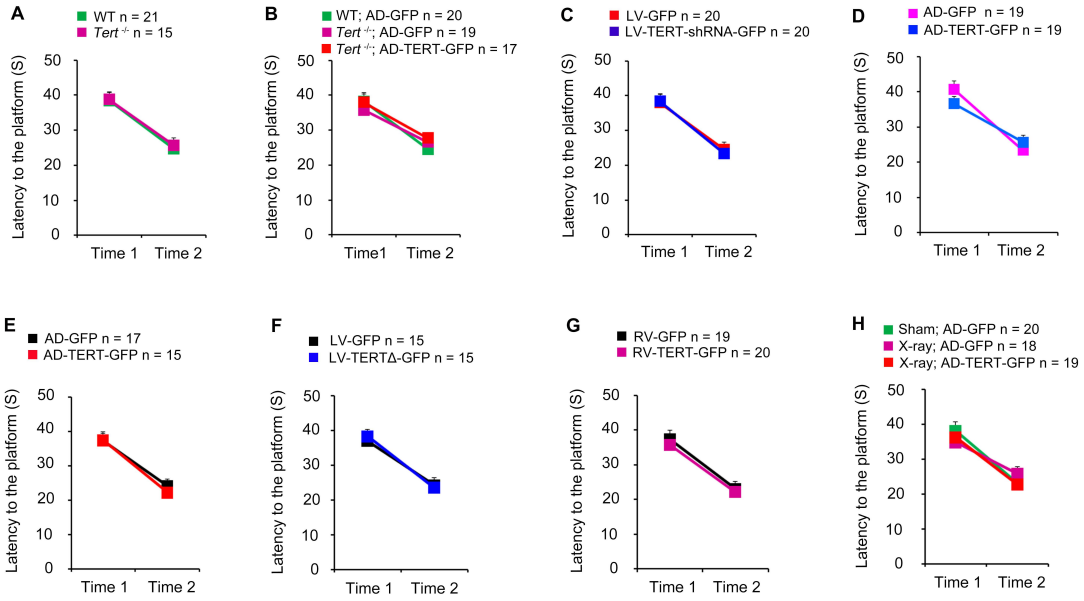

Figure S3. TERT expression dynamic induced by AD-TERT-GFP. Related to Figure 2

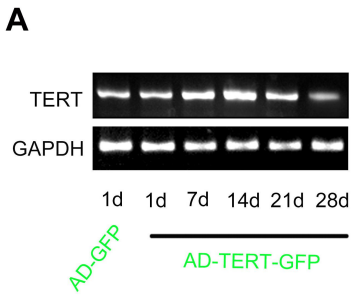

Figure S4. Validation of RV-TERT-GFP *in vivo* and *in vitro*. Related to Figure 4

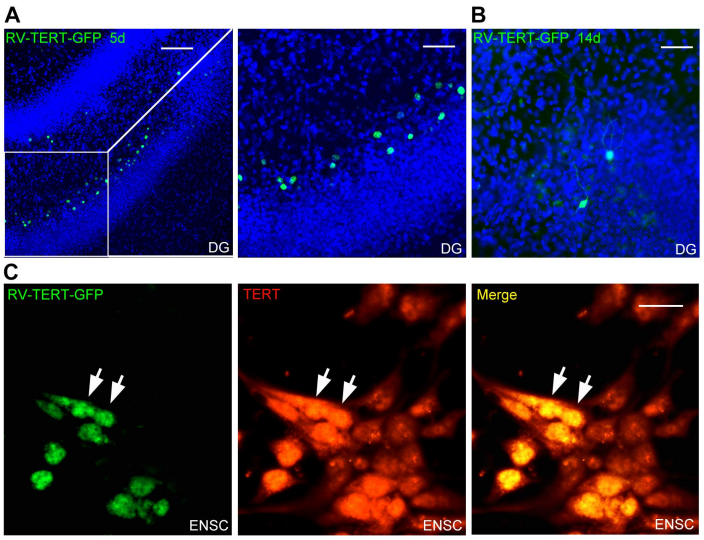

Figure S5. Cell types of LV-TERT-GFP infected cells in the DG. Related to Figure 7

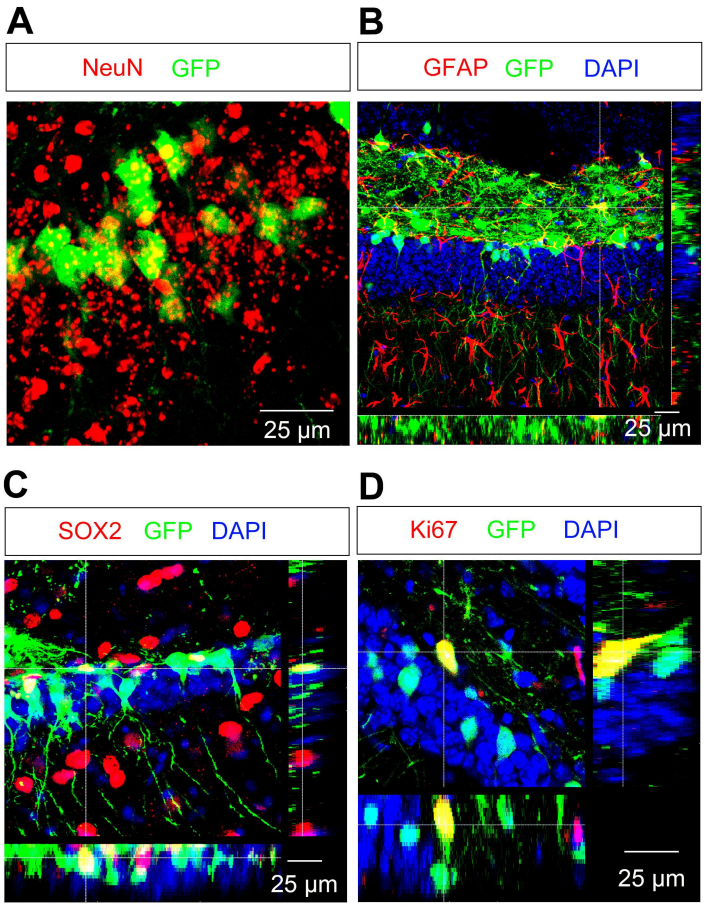

Figure S6. X ray-irradiation causes cell death selectively in the sub-granular layer of the DG. Related to Figure 7

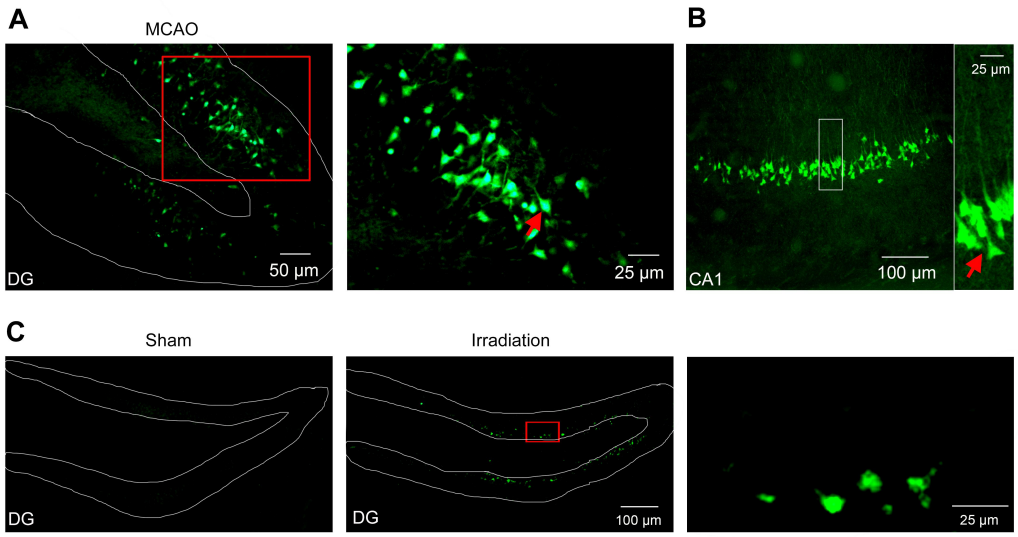

Figure S7. Expression of shortened TERT with non-activity in the DG did not cause depression-related behavior. Related to Figure 6

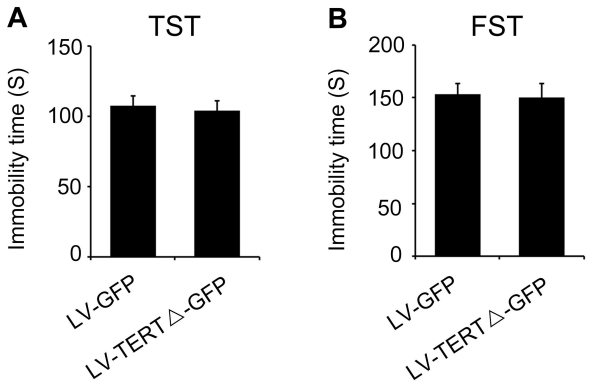

Table S1. The swimming speeds in probe test of mice in each experiment. Related to Figure 1, 2, 6 and 7

Experiments	Groups	n	Swim speed (mm/s) Mean ± SEM	*P* value
Figure 1**A**	WT	21	507.4667 ± 14.9994	0.2199
	Tert$^{-/-}$	15	479.3620 ± 16.3210	
Figure 1**E**	WT;LV-GFP	20	445.1270 ± 15.7291	0.2430
	Tert$^{-/-}$;LV-GFP	19	451.6412 ± 18.0740	
	Tert$^{-/-}$;LV-TERT-GFP	17	413.9472 ± 15.7541	
Figure 1**H**	LV-GFP	20	431.5740 ± 12.4375	0.5923
	LV-TERT-shRNA-GFP	20	420.2310 ± 16.9280	
Figure 2**A**	AD-GFP	19	452.5030 ± 22.5279	0.7358
	AD-TERT-GFP	19	442.1970 ± 20.2784	
Figure 2**B**	AD-GFP	17	457.2770 ± 9.8820	0.2354
	AD-TERT-GFP	15	441.4620 ± 15.3795	
Figure 6**E**	LV-GFP	15	439.3920 ± 10.4737	0.1592
	LV-TERTΔ-GFP	15	447.8219 ± 12.3251	
Figure 7**A**	RV-GFP	19	467.9337 ± 15.2172	0.3116
	RV-TERT-GFP	20	489.0720 ± 13.5414	
Figure 7**D**	Sham + AD-GFP	20	458.0568 ± 12.9293	0.8916
	X ray + AD-GFP	18	477.3935 ± 15.0006	
	X ray + AD-TERT-GFP	19	484.0584 ± 16.8535	

Movie S1. Related to Figure 1

This movie showed the performance of a mouse in WT group in MWM test at day 5 during 5-day training. The WT mouse found the platform in a short time.

Movie S2. Related to Figure 1

This movie showed the performance of a mouse in *Tert*$^{-/-}$ group in MWM test at day 5 during 5-day training. The *Tert*$^{-/-}$ mouse did not found the platform.

Supplemental Figure Legends

Figure S1. Validation of the *Tert* $^{-/-}$ mice (related to Figure 1). (**A**) RT-PCR showing the genotype of the *Tert* $^{-/-}$ mice. (**B**) Deletion of telomerase activity in the embryonic stem cells from *Tert* $^{-/-}$ mice ($n = 3$ independent experiments, $P = 0.0012$, Student's t-test.). Error bars, s.e.m.

Figure S2. Latency to the platform in visible platform training (related to Figure 1, 2, 6 and 7). (A) Related to Figure 1A. (**B**) Related to Figure 1E. (**C**) Related to Figure 1H. (**D**) Related to Figure 2A. (**E**) Related to Figure 2B. (**F**) Related to Figure 6E. (**G**) Related to Figure 7A. (**H**) Related to Figure 7D. One-way ANOVA in (**B** and **G**) and Student's *t*-test in the others. Error bars, s.e.m.

Figure S3. TERT expression dynamic induced by AD-TERT-GFP (related to Figure 2). (**A**) RT-PCR showing the expression dynamic of TERT mRNA after injection of AD-TERT-GFP into the DG. $n = 3$ independent experiments.

Figure S4. Validation of RV-TERT-GFP *in vivo* and *in vitro* (related to Figure 4). (**A**) Representative image of the DG infected by RV-TERT-GFP 5 days after RV infection. On the right: a high-magnification image from the box area, showing the location of RV-TERT-GFP in the sub-granular layer. (**B**) Representative image of the DG infected by RV-TERT-GFP 14 days after RV infection. Note that the major GFP fluorescence was observed in the cell body. (**C**) Representative image of the cultured NSCs infected by RV-TERT-GFP (left) with immunostaining with anti-TERT primary antibody (middle). The merge of RV-TERT-GFP signal with TERT immunostaining signal (yellow) was shown (right). Note: the signal of TERT in the NSCs infected by RV-TERT-GFP (arrow indicated) was significantly stronger than others, indicating an enhancement of TERT expression in NSCs by RV-TERT-GFP 24 hours after infection in NSCs culture. Scale bars: **A** (left), 100 μm; **A** (right) and **B**, 50 μm, **C**, 25 μm.

Figure S5. Cell types of LV-TERT-GFP infected cells in the DG (related to Figure 7). (**A**) Representative photo showing that NeuN^{+} neurons located at the granular layer were infected by LV-TERT-GFP. (**B**) Representative photo showing that GFAP^{+} astrocytes in the hillus were infected by LV-TERT-GFP. (**C**) Representative photo showing that SOX2^{+} cells located in the sub-granular layer were infected by LV-TERT-GFP. (**D**) Representative photo showing that Ki67^{+} cells located in the sub-granular layer were infected by LV-TERT-GFP.

Figure S6. X ray-irradiation causes cell death selectively in the sub-granular layer of the DG (related to Figure 7). (**A**) Representative photos showing FJ-positive cells located in the DG 7 days after MCAO. A magnification of the box area was shown on the right. Red arrow indicated that

FJ-positive cells located in the granular layer with neuronal morphology. (**B**) Representative photos showing FJ-positive cells located in the CA1 7 days after MCAO. A magnification of the box area was shown on the right. Red arrow indicated that FJ-positive cells located in the granular layer with neuronal morphology. (**C**) Representative photos showing FJ-positive cells in the DG of mice with/without exposure to irradiation. A magnification of the box area was shown on the right. Red arrow indicated that FJ-positive cells located in the granular layer with the morphology of NPCs. $n = 3$ independent experiments.

Figure S7. Expression of shortened TERT with non-activity in the DG did not cause depression-related behavior (related to Figure 6). (A) Bar graph showing the immobility time of mice in TST 28 days after injection of LV-GFP or LV-TERTΔ-GFP into the DGs. $n = 15$. $P = 0.7148$. Student's *t*-test. (B) Bar graph showing the immobility time of mice in FST 28 days after injection of LV-GFP or LV-TERTΔ-GFP into the DGs. $n = 15$. $P = 0.8810$. Student's *t*-test.

Supplemental Experimental Procedures

Genotyping

Genotyping Primers of *Tert*$^{-/-}$ mice: (1) gcg tgg agt atc ctc ctg cat ctc ta, (2) ctg tct cct aaa gga ctt gtg gac tt, (3) agg att ggg aag aca ata gca ggc at. The primer stock should be diluted to make 100 picomoles/ µl. Then mix 10 µl of each primer 1, 2, and 3 with 70 µl 3-distilled water to make final volume of 100 µl. This 100 µl is the working stock. 1 µl of the working stock can be used for 1 PCR reaction. PCR cycles: 32 cycles. Denaturation: 94 °C, 30 sec. Annealing: 55 °C, 30 sec. Extension: 72 °C, 1 min. Final extension: 72 °C, 10 min.

Virus construction

RV-TERT-GFP The sequence of TERT-GFP in the plasmid pDC315-TERT-GFP was cutted by using restriction enzymes and inserted into the plasimd pCAG-GFP (For RV-GFP) by T4 DNA ligase to replace the sequence of GFP in pCAG-GFP. GFP was fused to the C-terminal of TERT. The plasmid was named as pCAG-TERT-GFP, which was used to identify by DNA sequencing. Using 100µl Lipofectamine 2000, 293T cells were co-transfected with 22.5 µg of pCAG-TERT-GFP, 15 µg of pCMV-GP, and 7.5 µg of pCMV-VSVG to generate the recombinant retrovirus, RV-TERT-GFP. After 48 h, supernatant was harvested from 293T cells, filtered at 0.45 µ m, and pelleted by ultracentrifugation at 18000 × g for 2 h at 4 °C. After resuspension by PBS, serially diluted retrovirus was used to transduce 293T cells; 4 days later, labeled 293T cells were counted to calculate the viral titer (~ 2 × 107 transducing units/ml). As a control, we also generated a retroviral vector that expresses GFP (RV-GFP) or RFP (RV-RFP) alone.

AD-TERT-GFP Briefly, the coding sequence of mouse TERT was amplified by RT-PCR. The primer sequences were as follows: forward, 5'-GTAGAACGCAGATCGAAT-TCATGACCCGCGCTCCTCG-3'; reverse, 5 '-CCCTTGCTCACCATG-AATTCGTCCAAAATGGTCTGAAAGTC-3'. The PCR fragments and the pDC315-GFP plasmid were digested with EcoR I and ligated with T4 DNA ligase to produce pDC315-mTERT-IRES-GFP. The plasmid was used to trans-form competent DH5α Escherichia coli bacterial strains for identification. Using 100µl of Lipofectamine 2000 mixed with 50 µl of DMEM, HEK293 cells were cotransfected with 5 µg of the pDC315-GFP plasmid with a cDNA encoding mTERT and 5 µg of the pBHG lox ΔE1,3 Cre plasmid as a helper plasmid to generate the recombinant adenovirus, AD-TERT-GFP. After 8 d, supernatant was harvested from HEK293 cells. After 3 times the virus amplification, the supernatant was filtered at 0.45µm and purified using the Adeno-X Virus Purification kit. After resuspension, serially diluted adeno-virus was used to transduce HEK293 cells. Seven days later, labeled HEK293 cells were counted to calculate the viral titer (~ 2.5 × 10 10 pfu/ml). As a control, we also generated a adenoviral vector that expresses GFP alone (AD-GFP).

LV-TERT-GFP and LV-TERTΔ-GFP Briefly, the coding sequence of mouse TERT was amplified by RT-PCR. The primer sequences were as follows: forward, 5'-GTAGAACGCAGATCGAAT-TCATGACCCGCGCTCCTCG-3'; reverse, 5 '-CCCTTGCTCACCATG-AATTCGTCCAAAATGGTCTGAAAGTC-3'. The PCR fragments was cutted by restriction enzymes and inserted into the plasimd pCMV-GFP (For LV-GFP) by T4 DNA ligase to replace the sequence of GFP in pCMV-GFP. GFP was under control of another promotor pUbi. Mice mTERTΔ gene was amplified by our previous consructed plasmid LV-TERT-GFP carring the whole gene encoding TERT by deletion mutant PCR. The primer sequences were as follows: forward, 5'-GAGGATCCCCGGGTACCGGTCGCCACCATGACCCGCGCTCCTCGTTGCC-3'; reverse, 5 '-TCCTTGTAGTCCATACCGTCCAAAATGGTCTGAAAGTCTGTGCTTAG -3'. The PCR fragments and the pGV287-GFP plasmid were digested with Age 1 and BamH 1 and ligated with T4 DNA ligase to produce LV-TERTΔ-GFP. Using 100μl Lipofectamine 2000, 293T cells were co-transfected with 20 μg of pCMV-TERT-GFP, 10 μg of VSVG, 7.5 μg of RSV-REV and 3.5 μg pMDL g/p RRE to generate the recombinant lentiovirus, LV-TERT-GFP. After 48 h, supernatant was harvested from 293T cells, filtered at 0.45 μ m, and pelleted by ultracentrifugation at 18000 × g for 2 h at 4 °C. After resuspension by PBS, serially diluted retrovirus was used to transduce 293T cells; 4 days later, labeled 293T cells were counted to calculate the viral titer (~ 2 × 109 transducing units/ml). As a control, we also generated a retroviral vector that expresses GFP alone (LV-GFP).

LV-TERT-shRNA-GFP Mouse TERT shRNA (m) Lentiviral Particles, we named it LV-TERT-shRNA-GFP, and its control shRNA Lentiviral Particles (LV) were purchased (Santa Cruz, CA, USA). LV-TERT-shRNA-GFP is a pool of concentrated, transduction-ready viral pa rticles containing 4 target-specific constructs that encode 19- 25 nt (plus hairpin) shRNA designed to knock down gene expression. Each vial contains 200 μl frozen stock containing 1.0 × 106 infectious units of virus (IFU) in Dulbecco's Modified Eagle's Medium with 25 mM HEPES pH 7.3.

RV-SYN-GTR, RV-SYN-GT, and EnvA-ΔR-mCh The plasmids of RV-SYN-GTR and RV-SYN-GT were constructed based on the plasmids from Callaway's lab purchased from addgene (Osakada and Callaway, 2013). RV-SYN-GTR and RV-SYN-GT were produced by transient transfection of the RV-SYN-GTR or RV-SYN-GT vector (7.5 μg), CMVGagPol (5 μg) and CMV-VSVG (2.5 μg) in 60% confluent 293T cells grown in 10-cm plates for 5 hours. Virus-containing supernatant was harvested 48 hours later. The final titers were estimated to be ~ 2 × 107 pfu/ml or ~ 1 × 107 pfu/ml as determined by infection of serially diluted virus into 293T cells. The production of EnvA-ΔR-mCh was carried out as described previously (Osakada and Callaway, 2013; Osakada et al., 2011). Briefly, glycoprotein–gene-deleted rabies virus vector (ΔR-mCherry) was generated in which a mCherry reporter gene was replaced with the cDNA encoding the rabies virus glycoprotein. The helper cell line, BHK-EnvARGCD, was infected with ΔR-mCherry, to produce rabies virus pseudotyped with envelope protein EnvA. After 2 h and 4 h, the cells were washed with PBS three times and the media

reapplied. Supernatants containing ΔR-mCherry rabies virus pseudotyped with EnvA were harvested 5 days later, filtered and concentrated by ultracentrifugation. EnvA-ΔR-mCh titre was estimated to be ~1.2×107 pfu/ml and diluted for use to ~4×106 pfu/ml.

Western blot

Western bolt analysis of samples from cultured hippocampal neurons, NSC, and hippocampal tissues of animals was performed as described previously (Zhou et al., 2011b). The primary antibodies: Rabbit Anti-Flag (Bioss, bs-0287R), Mouse Anti-GAPDH (Kangchen Bio-Tech, kc-5G4), and Rabbit Anti-Synapsin 1 (Millipore, AB1543). Appropriate horseradish peroxidase-linked secondary antibodies were used for detection by enhanced chemiluminescence (Pierce).

MCAO

Focal cerebral ischemia was induced by MCAO, as described previously (Zhou et al., 2010). In brief, under chloral hydrate anesthesia (350 mg/kg, i.p.), a 8/0 surgical nylon monofilament with rounded tip was introduced into the left internal carotid artery through the external carotid stump, advanced 16–17 mm past the carotid bifurcation until a slight resistance was felt. At this point, the intraluminal filament blocked the origin of the middle cerebral artery and occluded all sources of blood flow from the internal carotid artery, anterior cerebral artery, and posterior cerebral artery. Throughout the procedure, body temperature was maintained at 37 ± 0.5 °C. The filament was left in place for 90 min and then withdrawn. In the sham-operated animals, the occluding filament was inserted 7 mm above the carotid bifurcation.

Fluoro-Jade staining

Neuronal degeneration and death were determined by Fluoro-Jade (FJ; Histo-Chem) staining (Zhou et al., 2011a). In brief, sections were washed and mounted on glass slides and dried overnight. The slides were immersed for 3 min in absolute ethanol solution, for 1 min in 70% ethanol solution, and for 1 min in distilled water. Then, the slides were transferred into a solution containing 0.01% Fluoro-Jade and 0.1% acetic acid for 30 mintues on a shaker. After three 10 mintues washes, the slides were finally coverslipped for analysis.

Immunocytochemistry

Mice were anesthetized with with 0.07 ml of a mixture of ketamine (90.9 mg/ml) and xylazine (9.1 mg/ml) and perfused transcardially with saline followed by about 50 ml of 4% paraformaldehyde (PFA). Brains were removed and postfixed overnight in 4% PFA. Serial sections (40μm) were made on an oscillating tissue slicer in a bath of physiological saline. Every sixth section throughout the hippocampus was processed for 5-bromo-2′-deoxyuridine (BrdU) (Rat, Bio-rad, OBT0030) immunohistochemistry as described previously. All the sections throughout the brain were collected

for tracing analyis. All the cells were counted in each section by another experimenter blinded to the study code. Other primary antibodies: Rabbit Anti-DCX (Santa Cruz Biotechnology, sc-28939), Rabbit Anti-GFAP (Abcam, ab7260), Mouse Anti-GFP (Santa Cruz Biotechnology, sc-101525), Rabbit Anti-RFP (Abcam, ab62341), Rabbit Anti-Ki67 (Abcam, ab66155), Rabbit Anti-SOX2 (Abcam, ab97959), Rabbit Anti-NeuN (Cell Signaling, #24307), and Rabbit Anti-Synapsin 1 (Millipore, AB1543).

RT-PCR

Total mRNA was extracted from the hippocampus using Trizol reagent according to the manufacturer's instructions (Sigma). The primers used for RT-PCR: TERT: forward, 5' –ATGGCGTTCCTGAGTATG – 3', reverse, 5' –AGCCAGAGGCCTTTAGT – 3'; GAPDH: forward, 5' – CAAGGTCATCCATGACAACTTTG – 3', reverse, 5' – GTCCACCACCCTGTTGCTGTAG - 3'. PCR conditions were 30 cycles of denaturation at 94°C for 45 s, annealing at 55°C for 45 s, and extension at 72°C for 45 sec. PCR products were separated by electrophoresis through 1.5% agarose gel containing 0.5% lg/mL ethidium bromide and imaged using a BioDoc-IT imaging system (Bio-Rad); band intensities were determined using GS-710 calibrated imaging Densitometer (Bio-Rad). The mRNA for GAPDH was detected as a standard.

Telomerase activity assay

Telomerase activity was detected using TRA-PEZE XL telomerase detection kit (Millipore, Billerica, MA) as described previously (Zhou et al., 2011a). Following the manufacturer's instructions, telomeric repeat amplification protocol reactions (TRAP) were performed using the TRAPEZE XL telomerase detection kits (Millipore) for analysis of the telomerase activity. The fluorescence energy transfer primers were used to generate fluorescently labeled TRAP products, quantitatively measured with a fluorescence plate reader (SpectraMax M2e) or visualized after terminal deoxynucleotidyl transferase-mediated dUTP nickend labeling on a 10% nondenaturing gel and SYBR Green I (Invitrogen) staining.

Analysis of spine density and morphology of neurons

Images of GFP-labeled neurons or DCX^+ neurons were acquired at 1 μm intervals with the Leica confocal system with a plane apochromatic 40 × oil lens and a digital zoom of 1.5. The image files were used for reconstruction of the morphology with the Imaris v7.2.3 program. The length of each dendritic segment was determined by tracing the center of the dendritic shaft, and the number of spines was counted manually from the two-dimensional projections. The linear spine density was calculated by dividing the total number of spines by the length of the dendritic segment. For classification of mushroom spines, major and minor axes of each spine head were identified. When the

width size of the spine > 0.6 μm, the spines regonized as mushroom spines. Confocal imaging and data quantification were done by the same person, who was blinded to the experimental conditions.

Stereotaxic surgery

Mice were anesthetized with 0.07 ml of a mixture of ketamine (90.9 mg/ml) and xylazine (9.1 mg/ml) and placed in a stereotaxic apparatus. Stereotaxic surgery was performed to deliver viruses or drugs into the hippocampal DG (1 μl, coordinates: 2.3 mm posterior to bregma, 1.35 mm lateral to the midline, and 2.3 mm below dura), The mice were recoverd on hot pad (37 °C) until waken up and then retrun back to homecages (Zhou et al., 2011).

Hippocampal X-irradiation

As described previously (Zhou et al., 2011), X-irradiation was performed. Briefly, mice were anesthetized with 0.07 ml of a mixture of ketamine (90.9 mg/ml) and xylazine (9.1 mg/ml). Then mice were placed in a stereotaxic apparatus and the hippocampal zone were exposed to cranial irradiation using therapeutical x-ray equipment operated at 300 kVp and 20 mA. Mice were protected with a lead shield that covered the entire body, with the exception of a 3.2 × 11 mm treatment field above the hippocampus. The corrected dose rate was ≈ 3 Gy/min at a source-toskin distance of 100 cm. The procedure lasted 1 min and 42 s, delivering a total of 5 Gy each time.

Cell Cultures

Primary hippocampal neurons were cultured from embryonic hippocampus, on embryonic day 18 (E18), of WT or *Tert*$^{-/-}$ mice in neurobasal medium (Gibco) containing 2% B27 supplement as reported (Luo et al., 2010). NSCs differentiation was also performed from embryonic hippocampus on embryonic day 18 (E18), of WT or *Tert*$^{-/-}$ mice. Monolayer-cultured NSCs were allowed to differentiate in growth factor-free DMEM/F12 (1:1) medium containing 2% B27 and 0.5% fetal bovine serum. Four days later, the cultures were fixed and stained with DCX and GFAP antibodies to mark neurons and astrocytes, respectively. The percentages of neurons and astrocytes were calculated in 10 high-power fields systematically across the coverslip.

Supplemental References

Luo, C.X., Jin, X., Cao, C.C., Zhu, M.M., Wang, B., Chang, L., Zhou, Q.G., Wu, H.Y., and Zhu, D.Y. (2010). Bidirectional regulation of neurogenesis by neuronal nitric oxide synthase derived from neurons and neural stem cells. Stem cells *28*, 2041-2052.

Osakada, F., and Callaway, E.M. (2013). Design and generation of recombinant rabies virus vectors. Nature protocols *8*, 1583-1601.

Osakada, F., Mori, T., Cetin, A.H., Marshel, J.H., Virgen, B., and Callaway, E.M. (2011). New rabies virus

variants for monitoring and manipulating activity and gene expression in defined neural circuits. Neuron *71*, 617-631.

Zhou, L., Li, F., Xu, H.B., Luo, C.X., Wu, H.Y., Zhu, M.M., Lu, W., Ji, X., Zhou, Q.G., and Zhu, D.Y. (2010). Treatment of cerebral ischemia by disrupting ischemia-induced interaction of nNOS with PSD-95. Nature medicine *16*, 1439-1443.

Zhou, Q.G., Hu, Y., Wu, D.L., Zhu, L.J., Chen, C., Jin, X., Luo, C.X., Wu, H.Y., Zhang, J., and Zhu, D.Y. (2011a). Hippocampal telomerase is involved in the modulation of depressive behaviors. The Journal of neuroscience : the official journal of the Society for Neuroscience *31*, 12258-12269.

Zhou, Q.G., Zhu, L.J., Chen, C., Wu, H.Y., Luo, C.X., Chang, L., and Zhu, D.Y. (2011b). Hippocampal neuronal nitric oxide synthase mediates the stress-related depressive behaviors of glucocorticoids by downregulating glucocorticoid receptor. The Journal of neuroscience : the official journal of the Society for Neuroscience *31*, 7579-7590.